Fractional Superlets

Harald Bârzan
Transylvanian Institute of Neuroscience
Technical University of Cluj-Napoca
Cluj-Napoca, Romania
barzan@tins.ro

Vasile V. Moca
Transylvanian Institute of Neuroscience
Cluj-Napoca, Romania
moca@tins.ro

Ana-Maria Ichim
Transylvanian Institute of Neuroscience
Technical University of Cluj-Napoca
Cluj-Napoca, Romania
ichim@tins.ro

Raul C. Mureşan
Transylvanian Institute of Neuroscience
Cluj-Napoca, Romania
muresan@tins.ro

***Abstract*—The Continuous Wavelet Transform (CWT) provides a multi-resolution representation of a signal by scaling a mother wavelet and convolving it with the signal. The scalogram (squared modulus of the CWT) then represents the spread of the signal's energy as a function of time and scale. The scalogram has constant relative temporal resolution but, as the scale is compressed (frequency increased), it loses frequency resolution. To compensate for this, the recently-introduced *superlets* geometrically combine a set of wavelets with increasing frequency resolution to achieve time-frequency super-resolution. The number of wavelets in the set is called the order of the *superlet* and was initially defined as an integer number. This creates a series of issues when adaptive *superlets* are implemented, i.e. *superlets* whose order depends on frequency. In particular, adaptive *superlets* generate representations that suffer from "banding" because the order is adjusted in discrete steps as the frequency increases. Here, by relying on the weighted geometric mean, we introduce fractional *superlets*, which allow the order to be a fractional number. We show that fractional adaptive *superlets* provide high-resolution representations that are smooth across the entire spectrum and are clearly superior to representations based on the discrete adaptive *superlets*.**

Keywords—continuous wavelet transform, scalogram, superlet transform, adaptive superlets

I. Introduction

Wavelets are among the most popular tools used for constructing time-scale representations of signals [1]–[3]. These are scaled versions of a "mother wavelet", which is necessarily the impulse response of a band-pass filter, having zero mean. Wavelets act as constant-Q band-pass filters [4]–[6]. The mother wavelet has a characteristic, central frequency, which is then decreased / increased by scaling. To construct a time-scale representation, one convolves the signal with a family of scaled wavelets, spanning a range of scales (frequencies). The operation is called a "Continuous Wavelet Transform" (CWT) [7]. The squared modulus of the CWT is called a *scalogram* [2].

On the other hand, the *spectrogram* is a very popular tool for constructing time-frequency representations [8]. This is computed by taking the squared modulus of the Short-Time Fourier Transform (STFT) [5]. The spectrogram belongs to the family of bilinear quadratic representations and is obtained by smoothing the Wigner-Ville Distribution (WVD) of the signal with the WVD of the window [2].

The scalogram is a representation fundamentally different from the spectrogram, although a correspondence between the two can be easily established [5]. If one considers the representation as a set of time-frequency Heisenberg uncertainty boxes [4], for the spectrogram these boxes have a constant shape, irrespective of the time and frequency location in the representation. By contrast, in the scalogram the temporal size of the boxes is compressed while their frequency extent is expanded as one ascends in frequency. This happens because, with increasing frequency, an increasing number of oscillation cycles fit into the spectrogram's window, while the number of cycles are constant for the scalogram, because the wavelet is progressively compressed [2]. In other words, the spectrogram maintains frequency resolution at the expense of relative temporal resolution, while the scalogram maintains relative temporal resolution at the expense of frequency resolution.

The ability of the scalogram to "adapt" to each analyzed frequency by scaling the mother wavelet is called "multi-resolution" or "multiscale". Unfortunately, the latter comes at a cost: the frequency resolution of the scalogram degrades progressively with the decrease (compression) in scale (increase in frequency). To solve this problem, a recent method has been proposed, which replaces a single scalogram with the geometric combination of a set of scalograms. For a certain central frequency, the *superlet* uses a set of wavelets with the same central frequency but progressively narrower bandwidths (longer, with more cycles). It then combines these geometrically in order to maintain the good temporal precision of short wavelets and gain the good frequency precision of long wavelets [9]. This follows an idea similar to minimum mean cross-entropy (MMCE) method, which computes the geometric mean of spectrograms with different resolutions (window sizes) [10], [11]. The MMCE has been shown to be the closest to the set of spectrograms with respect to an entropic criterion [11]. The MMCE however is not a multiscale method. It therefore suffers from a "dilution" effect for oscillation packets with constant number of cycles which become narrower in time as their frequency increases. Unlike the MMCE, *superlets* do not suffer from the dilution effect [9].

Analogous to the CWT, one can compute the *superlet* transform (SLT), which creates a representation of the signal by using a set of mother wavelets with different bandwidths, convolving their scaled versions with the signal, and geometrically combining the latter. The *superlet* scalogram is then computed as the squared modulus of the SLT [9].

This work was supported by a grant from the Romanian National ~~Authority for Scientific Research and Innovation, CNCS-UEFISCDI~~ (COFUND-NEURON-NMDAR-PSY), a project co-funded by the European Social Fund (Entrepreneurial competences and excellence research in doctoral and postdoctoral programs – ANTREDOC), and a National Science Foundation grant NSF-IOS-1656830 funded by the US Government. Any opinions, findings, and conclusions or recommendations expressed in this material are those of the authors and do not necessarily reflect the views o the National Science Foundation.

The number of mother wavelets in the set of a *superlet* is called the "order" of the *superlet* [9]. The CWT is a special case of SLT, where the order parameter is 1. The larger the order, the more the *superlet*'s response is constrained in frequency (less redundancy, narrower band-pass characteristics) [9]. In general, in the CWT, low-frequency components are already well localized in frequency, while their frequency localization degrades progressively with increasing frequency. Therefore, one would like to use a lower order in the SLT for low frequencies and a higher order for high frequencies. This is called the "adaptive *superlet* transform" (ASLT).

The problem of the ASLT in its original formulation [9] is that the order is an integer number (representing the number of wavelets in the *superlet*) and it is increased from low to high in discrete steps. This produces an annoying "banding" of the representation. Here, we solve this problem by introducing a generalization of the *superlet* to a geometrically fractional weighted form. We show that the ASLT scalograms based on the fractional *superlet* are vastly superior to the discrete ASLT, on both synthetic data and signals recorded from the brains of animals (*in vivo* electrophysiology) and humans (electroencephalography–EEG).

II. Methods

A. From wavelets to superlets

A wavelet is the impulse response of a band-pass filter, and it is obtained by scaling a "mother" wavelet function:

$$\psi(t,a) = \frac{1}{a}\psi_m\left(\frac{t}{a}\right) \tag{1}$$

Here we use the $1/a$ scaling of the wavelet such that the integrated modulus of the scaled version equals that of the mother wavelet. This type of normalization is especially used for wavelet ridge detection [4], [12] and can be shown to converge to the instantaneous power of a tone signal when the scale (frequency) of the wavelet is matched to the tone's frequency.

The CWT of a signal x then becomes:

$$\begin{aligned} CWT_x(t,a) &= \frac{1}{a}\int_{-\infty}^{\infty} x(\tau)\,\psi_m^*\left(\frac{\tau - t}{a}\right)d\tau \\ &= \int_{-\infty}^{\infty} x(\tau)\,\psi(\tau - t, a)d\tau \end{aligned} \tag{2}$$

where, a is the scale and ψ_m is the mother wavelet. Since the mother wavelet has a characteristic central frequency, ω_m [2], one can express the CWT as a function of frequency by replacing the scale, a, with the inverse of frequency, ω_a:

$$a = \frac{\omega_m}{\omega_a} \tag{3}$$

The CWT then becomes:

$$CWT_x(t,\omega_a) = \frac{\omega_a}{\omega_m}\int_{-\infty}^{\infty} x(\tau)\,\psi_m^*\left[\frac{\omega_a(\tau - t)}{\omega_m}\right]d\tau \tag{4}$$

and the scalogram is:

$$T_x(t,\omega_a) = |CWT_x(t,\omega_a)|^2 \tag{5}$$

As the frequency, ω_a, is increased (a is decreased), the wavelet is compressed in time while its band-pass characteristic widens in frequency. The band-pass characteristic of the scaled wavelets depends primarily on the band-pass characteristic of the mother wavelet: the longer in time the mother wavelet (more cycles at ω_m), the narrower the frequency response of all the wavelets derived from it, and *vice versa*. The mother wavelet therefore has two parameters: ω_m and c_m, where c_m is a design parameter which sets the number of cycles at its central frequency, ω_m. Operating in angular frequency, the popular modified Morlet [13] mother wavelet can be defined as:

$$\psi_m(\omega_m, c_m; t) = \frac{1}{\sigma_m\sqrt{2\pi}}e^{-\frac{1}{2}\left[\frac{t}{\sigma_m}\right]^2}e^{j\omega_m t} \tag{6}$$

$$\sigma_m = \frac{2\pi c_m}{5} \tag{7}$$

where, σ_m is a time-spread parameter chosen such that the plane sinusoidal wave spans c_m cycles (periods) within $5\sigma_m$.

Longer mother wavelets (larger c_m) ensure the CWT is more precise in frequency but less precise in time, while shorter mother wavelets (smaller c_m) provide better temporal precision but worse frequency resolution.

Since ω_m is arbitrary, we can set it to 1, without loss of generality. The child wavelets then become:

$$\psi(c_m; t, \omega) = \frac{5\omega}{c_m(2\pi)^{\frac{3}{2}}}e^{-\frac{1}{2}\left[\frac{5\omega t}{2\pi c_m}\right]^2}e^{j\omega \mathrm{t}} \tag{8}$$

The *superlet* combines wavelets with small c_m with those having larger c_m to achieve time-frequency super-resolution [9]. The standard setting is where a base number of cycles, c_1 is scaled multiplicatively across the wavelet set. Considering the child wavelet formula in (8), the *superlet* transform of a signal, x, is defined as:

$$SLT_{x,c_1,o}(t,\omega) = \prod_{i=1}^{o}[R_x(c_1 \cdot i; t, \omega)]^{\frac{1}{o}} \tag{9}$$

where, o is the order of the *superlet*, defining the number of wavelets that compose it, and $R_x(c_i; t,\omega)$ is computed by the convolution of the wavelet with c_i cycles with the signal, x:

$$R_x(c_i; t, \omega) = \sqrt{2}\int_{-\infty}^{\infty} x(\tau)\,\psi(c_i; \tau - t, \omega)d\tau \tag{10}$$

When $o = 1$, the SLT is equivalent to the CWT. For larger orders, the SLT concentrates frequency response, maintaining temporal resolution. The $\sqrt{2}$ term is added only for analytical (complex) wavelets, such as the Morlet, in order to recover the full power from the spectrum of real signals.

The *superlets* scalogram is then defined as:

$$L_{x,c_1,o}(t,\omega) = \left|\mathrm{SLT}_{x,c_1,o}(t,\omega)\right|^2 \tag{11}$$

The base cycles parameter, c_1, controls the temporal resolution of the representation and is usually taken in the range 1-3. The order parameter, o, increases frequency resolution: the higher its value, the more concentrated the representation is in frequency, with less redundancy for the higher frequencies [9].

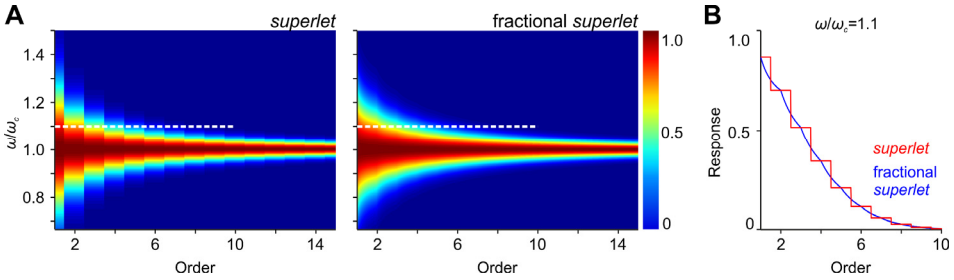

Figure 1. The normalized responses of the *superlet* and fractional *superlet* to a tone (sine wave) as a function of order and relative frequency of the tone (ω/ω_c). A. The normalized response of the *superlet* (left) and fractional *superlet* (right) to a tone at frequency ω/ω_c as a function of relative frequency and order. B. A section of the responses in (A) – white line, at $\omega=1.1\cdot\omega_c$ shows the exact profiles of the *superlet* (red) and fractional *superlet* (blue). The central frequency of the *superlet* and fractional *superlet* is ω_c.

B. *Adaptive superlets*

In the scalogram, the frequency resolution degrades with increasing frequency. Therefore, it is desirable to concentrate the frequency bandwidth progressively, as one ascends in frequency. This is achieved by the adaptive *superlet* transform (ASLT), where the order is linearly increased from the lowest to the highest frequency:

$$o(\omega) = o_{min} + round\left[(o_{max} - o_{min}) \cdot \frac{\omega - \omega_{min}}{\omega_{max} - \omega_{min}}\right] \quad (12)$$

where, ω_{min} and ω_{max} are, respectively, the smallest and largest frequency in the representation, and o_{min} and o_{max} are the orders chosen for these two extremes of the spectrum.

In the definition of the *superlet* from eq. (9), the order is an integer number, such that the formula in eq. (12) produces abrupt jumps of the order as the frequency is increased. This creates a "banding" of the representation as the order increases in discrete steps with increasing frequency.

C. *Fractional superlets*

Here, we introduce the concept of "fractional superlets", which can take orders that are not integer numbers. We rely on the definition of the weighted geometric average and consider that each wavelet in the set corresponding to the integer part has a weight of 1, whereas the last one, if present, has a weight that corresponds to the fractional part. Let us define a "fractional order" as:

$$o_f = o_i + \alpha \quad (13)$$

where, o_f is a fractional order, composed of an integer order, $o_i \geq 1$, and a fractional part, $\alpha \in [0,1)$.

The fractional *superlet* transform is defined as:

$$FSLT_{x,c_1,o_f}(t,\omega) = \left[R_x(c_1[o_i+1];t,\omega)^{\alpha}\prod_{i=1}^{o_i} R_x(c_1\cdot i;t,\omega)\right]^{\frac{1}{o_f}} \quad (14)$$

In short, the FSLT includes a factor to the geometric mean that is weighted with the fractional part of the order. When α is 0, the FSLT is the same as the SLT.

D. *Adaptive fractional superlets*

Using the fractional *superlets*, one does not need to constrain the order of the ASLT to integer numbers anymore. The fractional ASLT (FASLT), simply uses the true fractional order, as:

$$o_f(\omega) = o_{min} + (o_{max} - o_{min}) \cdot \frac{\omega - \omega_{min}}{\omega_{max} - \omega_{min}} \quad (15)$$

For the SLT, the fractional order is in practice rarely necessary. However, as we will show next, it is very useful for the adaptive *superlets*.

III. Results

Next, we studied how the *superlet* and fractional *superlet* responded to a long sine wave (tone) as a function of the latter's frequency relative to the central frequency (ω_c) of the (fractional) *superlet* and its order. As the order was increased both the *superlet* and the fractional *superlet* limited their responses to tones close to their central frequency, as expected (Figure 1A).

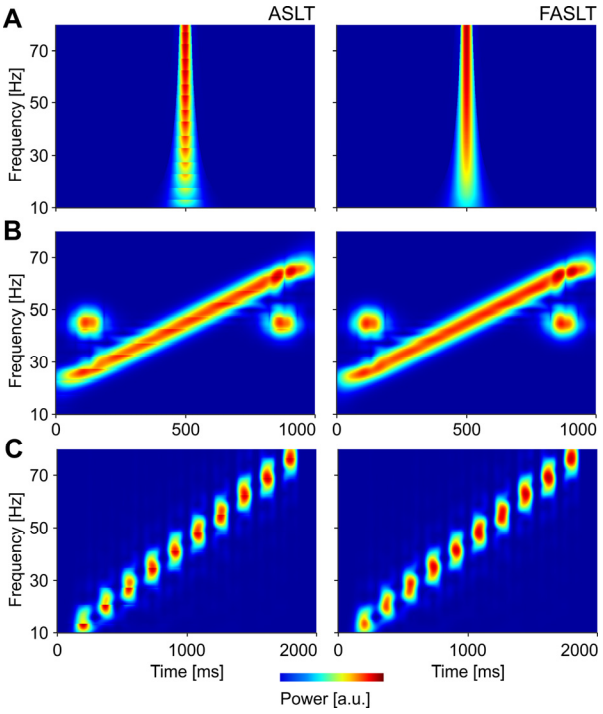

Figure 2. Discrete ASLT (left column) and FASLT (right column) representations on multiple synthetic data examples. A. Unit impulse. B. Linear FM chirp (20-70 Hz) engulfing two Gaussian atoms at 45 Hz. C. 100-millisecond long sinusoidal packets placed at the order crossings of the discrete ASLT. All representations were computed using an order interval of [1,11] and c_1=3.

Furthermore, as the order was increased the response was banded for the original *superlet* (due to discrete jumps in the order), while it was smooth for the fractional *superlet*. As the order was increased the banding issue of the *superlet* seemed

less severe, given that the representation at successive orders was already very concentrated. A section at one frequency near the central frequency, $1.1 \cdot \omega_c$, revealed that the fractional *superlet* was not completely smooth either: jumps are visible at points where the order is changed (Figure 1B). This effect however is rather small and hardly visible at low orders.

We next computed *superlets* scalograms based on the ALST and FASLT for synthetic signals, which contain known components, and for real-world data recorded in animal models (*in vivo* electrophysiology) and in humans (EEG).

A. Synthetic signals

To illustrate the problem FASLT is meant to solve, we first compared the ASLT and FASLT on a few synthetic examples (Figure 2). Although, this type of data is not frequently encountered in the real world, they serve well for illustrative purposes. All the synthetic examples were instances where the signal spanned wide frequency intervals over which the order of the ASLT varied. At the frequencies where the discrete order was increased, banding affected the ASLT representation (Figure 2, left). By contrast, in the FASLT the order varied smoothly, and the representation was also smooth (Figure 2, right).

B. In vivo electrophysiology data

The *in vivo* electrophysiological data was recorded from anesthetized mice during a visual perception task. Visual stimuli consisted of drifting sinusoidal gratings [14], [15]. During stimulus presentation gratings with a particular orientation (4 orientations between 0-180º in steps of 45º) were drifted along the screen in a particular, orthogonal direction, yielding 8 different drifting directions corresponding to the 4 orientations. Such stimuli are known to produce a robust entrainment of the primary visual cortex [16], typically inducing oscillatory activity in the gamma band (30-120 Hz) [17]. A 32-channel linear silicon probe (Neuronexus A32) was inserted into primary visual cortex (V1) of anesthetized mice and extracellular electrical activity was recorded during the visual stimulation session. Stimuli were presented monocularly on a Beetronics 12VG3 12 inch LED monitor with a resolution of 1440×900px. Extracellular data was then filtered (300Hz low-pass filter, Butterworth order 3 IIR, bidirectional) to obtain the local-field potential (LFP), which was downsampled to 1 kSamples/s.

LFP data shows well localized, short bursts of strong gamma oscillations. These are typical cases of brief gamma packets. A short window was required to resolve such short bursts with the STFT (spectrogram), resulting in poor frequency localization (Figure 3A). The same was true for the CWT (scalogram): good temporal resolution came at the expense of frequency resolution (Figure 3B). The ASLT on the other hand, was able to achieve high resolution in both time and frequency, albeit with its specific banding (Figure 3C). The FASLT solved this issue (Figure 3D), providing the best representation.

C. Electroencephalography data

Electroencephalography (EEG) data was recorded from human subjects during a visual pattern recognition task. The experiment consisted in presenting lattices of dots, deformed to resemble the contours of known objects [18]. Participants had to freely explore these stimuli and report whether or not they recognized the displayed objects. Their EEG data was simultaneously recorded with 128 electrodes, at a sampling rate of 1024 samples/s, using a commercial EEG acquisition device (Biosemi ActiveTwo).

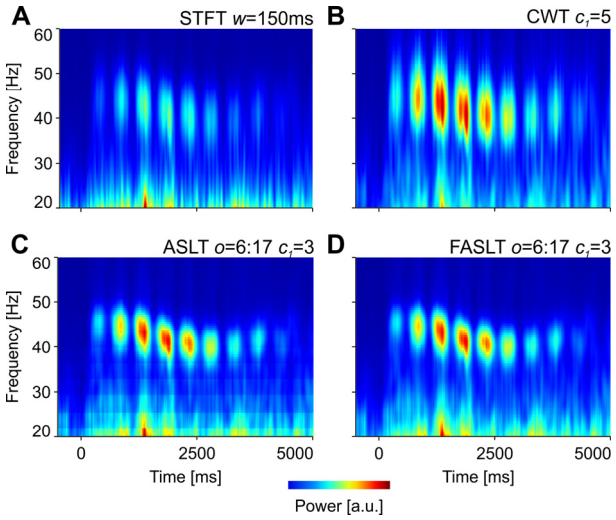

Figure 3. Gamma bursts in mouse visual cortex analysed with the STFT-spectrogram (A), CWT-scalogram (B), ASLT-scalogram (C), and FASLT-scalogram (D). The Blackman window was used for the STFT, and the modified Morlet wavelet for the CWT. The representations were computed as averages across all drifting directions.

Like intracranial electrophysiology recordings, the EEG data possesses a rich time-frequency structure, with many identifiable features. The key difference is that in the EEG there are multiple layers of complex tissue (scalp, skull bone, *dura mater*) between the recording electrodes and their intended target, which affect the acquired signal in multiple (possibly non-linear) ways. The most striking feature of this interference is the low-pass filter characteristic that attenuates high frequencies. As a result, it becomes increasingly harder for traditional time-frequency methods to adequately resolve EEG activity at higher frequencies.

Figure 4 depicts time-frequency representations of EEG data, recorded in our lab, from one subject. We compare two of the most commonly employed time-frequency representations, i.e., the spectrogram (STFT) and scalogram (CWT), with the discrete and fractional adaptive *superlets* (ASLT and FASLT). It is evident that many of the transient oscillatory bursts were missed by the standard methods. By contrast, *superlets* (in both forms) were able to properly identify high-frequency gamma bursts. The "banding" phenomenon described was also evident in the discrete ASLT, but not in the FASLT, which provided a smooth, high-frequency representation.

IV. Discussion

Superlets have been shown to provide excellent multi-scale time-frequency representations, overcoming the poor frequency resolution of the classical CWT [9]. When a relatively narrow frequency range is resolved, e.g. the gamma range (30-80 Hz) for electrophysiology data, the *superlet* transform (SLT) is sufficient for most applications. However, when a larger range of frequencies needs to be represented, the adaptive *superlet* transform (ASLT) is necessary [9]. The latter achieves a relatively constant frequency resolution throughout the representation.

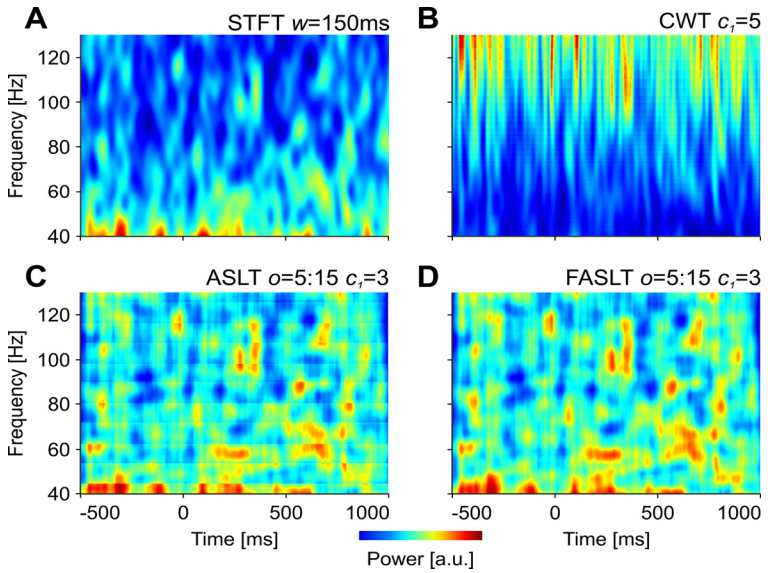

Figure 4. Time-frequency representations of EEG activity using the STFT-spectrogram (A), CWT-scalogram (B), ASLT-scalogram (C), and FASLT-scalogram (D). Data was recorded from the occipital lobe (electrode Oz) of a participant. The Blackman window was used for the STFT, and the modified Morlet wavelet for the CWT.

Here, we showed that the traditional ASLT produces banding in the representation due to the discrete, integer order of its underlying *superlets*. To solve this problem, we introduced the fractional *superlet*, whose order can be an arbitrary, fractional number. The fractional FASLT provides smooth representations that outperform the classical ASLT.

While the fractional *superlet* has a smoother response as a function of order, this is not entirely smooth, exhibiting small deviations around discrete order crossings. This deviation from smoothness has probably a very small impact on the representation. It remains a theoretical challenge to develop a fractional *superlet* whose response is completely smooth. This can probably be achieved by weighing the response of all the wavelets in the *superlet's* set.

V. ETHICS

The EEG protocol was approved by the Local Ethics Committee (1/CE/08.01.2018) and data was collected in accordance with Directive (EU) 2016/680 and Romanian Law 190/2018. *In vivo* experiments were approved by the Local Ethics Committee (3/CE/02.11.2018) and the National Veterinary Authority (147/04.12.2018). Datasets used here are available by email request from: muresan@tins.ro.

REFERENCES

[1] A. Teolis, *Computational Signal Processing with Wavelets*. Birkhäuser, 2017.

[2] O. Rioul and P. Flandrin, "Time-scale energy distributions: a general class extending wavelet transforms," *IEEE Transactions on Signal Processing*, vol. 40, no. 7, pp. 1746–1757, Jul. 1992, doi: 10.1109/78.143446.

[3] A. Grossmann and J. Morlet, "Decomposition of Hardy Functions into Square Integrable Wavelets of Constant Shape," *SIAM J. Math. Anal.*, vol. 15, no. 4, pp. 723–736, Jul. 1984, doi: 10.1137/0515056.

[4] S. Mallat, *A Wavelet Tour of Signal Processing: The Sparse Way*, 3 edition. Amsterdam ; Boston: Academic Press, 2008.

[5] B. Boashash, *Time-Frequency Signal Analysis and Processing: A Comprehensive Reference*. Academic Press, 2015.

[6] P. Flandrin and O. Rioul, "Affine smoothing of the Wigner-Ville distribution," in *International Conference on Acoustics, Speech, and Signal Processing*, Apr. 1990, pp. 2455–2458 vol.5, doi: 10.1109/ICASSP.1990.116088.

[7] A. Grossmann, R. Kronland-Martinet, and J. Morlet, "Reading and Understanding Continuous Wavelet Transforms," in *Wavelets*, Berlin, Heidelberg, 1990, pp. 2–20, doi: 10.1007/978-3-642-75988-8_1.

[8] L. Cohen, *Time-frequency Analysis*. Prentice Hall PTR, 1995.

[9] V. V. Moca, A. Nagy-Dăbâcan, H. Bârzan, and R. C. Mureşan, "Superlets: time-frequency super-resolution using wavelet sets," *bioRxiv*, p. 583732, Sep. 2019, doi: 10.1101/583732.

[10] S. Cheung and J. S. Lim, "Combined multiresolution (wide-band/narrow-band) spectrogram," *IEEE Transactions on Signal Processing*, vol. 40, no. 4, pp. 975–977, Apr. 1992, doi: 10.1109/78.127970.

[11] P. Loughlin, J. Pitton, and B. Hannaford, "Approximating time-frequency density functions via optimal combinations of spectrograms," *IEEE Signal Processing Letters*, vol. 1, no. 12, pp. 199–202, Dec. 1994, doi: 10.1109/97.338752.

[12] N. Delprat, B. Escudie, P. Guillemain, R. Kronland-Martinet, P. Tchamitchian, and B. Torresani, "Asymptotic wavelet and Gabor analysis: extraction of instantaneous frequencies," *IEEE Transactions on Information Theory*, vol. 38, no. 2, pp. 644–664, Mar. 1992, doi: 10.1109/18.119728.

[13] J. Morlet, G. Arens, E. Fourgeau, and D. Glard, "Wave propagation and sampling theory—Part I: Complex signal and scattering in multilayered media," *GEOPHYSICS*, vol. 47, no. 2, pp. 203–221, Feb. 1982, doi: 10.1190/1.1441328.

[14] O. F. Jurjuţ, M. Gheorghiu, W. Singer, D. Nikolić, and R. C. Mureşan, "Hold Your Methods! How Multineuronal Firing Ensembles Can Be Studied Using Classical Spike-Train Analysis Techniques," *Front. Syst. Neurosci.*, vol. 13, 2019, doi: 10.3389/fnsys.2019.00021.

[15] O. F. Jurjuţ, D. Nikolić, G. Pipa, W. Singer, D. Metzler, and R. C. Mureşan, "A Color-Based Visualization Technique for Multielectrode Spike Trains," *Journal of Neurophysiology*, vol. 102, no. 6, pp. 3766–3778, Oct. 2009, doi: 10.1152/jn.00758.2009.

[16] O. F. Jurjuţ, D. Nikolić, W. Singer, S. Yu, M. N. Havenith, and R. C. Mureşan, "Timescales of Multineuronal Activity Patterns Reflect Temporal Structure of Visual Stimuli," *PLOS ONE*, vol. 6, no. 2, p. e16758, Feb. 2011, doi: 10.1371/journal.pone.0016758.

[17] R. C. Mureşan, O. F. Jurjuţ, V. V. Moca, W. Singer, and D. Nikolić, "The oscillation score: an efficient method for estimating oscillation strength in neuronal activity.," *J Neurophysiol*, vol. 99, no. 3, pp. 1333–1353, Mar. 2008, doi: 10.1152/jn.00772.2007.

[18] V. V. Moca, I. Ţincaş, L. Melloni, and R. C. Mureşan, "Visual exploration and object recognition by lattice deformation.," *PLoS One*, vol. 6, no. 7, p. e22831, 2011, doi: 10.1371/journal.pone.0022831.